

Is the orbital-selective Mott phase stable against interorbital hopping?

Fabian B. Kugler¹ and Gabriel Kotliar^{1,2}

¹*Department of Physics and Astronomy, Rutgers University, Piscataway, NJ 08854, USA*

²*Condensed Matter Physics and Materials Science Department, Brookhaven National Laboratory, Upton, NY 11973, USA*

(Dated: December 30, 2021)

The localization-delocalization transition is at the heart of strong correlation physics. Recently, there is great interest in multiorbital systems where this transition can be restricted to certain orbitals, leading to an orbital-selective Mott phase (OSMP). Theoretically, the OSMP is widely studied for kinetically decoupled orbitals, but the effect of interorbital hopping remains unclear. Here, we show how nonlocal interorbital hopping leads to local hybridization in single-site dynamical mean-field theory (DMFT). Under fairly general circumstances, this implies that, at zero temperature, the OSMP, involving the Mott insulating state of one orbital, is unstable against interorbital hopping to another, metallic orbital. We further show that the coherence scale below which all electrons are itinerant is very small and gets exponentially suppressed even if the interorbital hopping is not overly small. Within this framework, the OSMP with interorbital hopping may thus reach down to extremely low temperatures T but not to $T = 0$. Accordingly, it is part of a coherence-incoherence crossover and not a quantum critical point. We present analytical arguments supported by numerical results using the numerical renormalization group as DMFT impurity solver. We also compare our findings with previous slave-spin studies.

The evolution of the electronic structure from localized to itinerant is a fundamental problem in condensed-matter physics and relevant to many interesting materials. It continues to receive much experimental attention as the transition region between localized and delocalized behavior hosts remarkable phenomena, such as high-temperature superconductivity [1–3].

Recently, there is a focus on multiorbital systems, triggered by the observation of orbital selectivity whereby a subset of orbitals (denoted “heavy”) has a much larger effective mass than another group (denoted “light”). An illustrative example under current study is $\text{FeTe}_{1-x}\text{Se}_x$ [4–7]. There, among the t_{2g} orbitals, the d_{xy} is the heaviest. A central idea in this field is the orbital-selective Mott phase (OSMP) [8] where the heavy electrons are Mott localized and coexist with the itinerant light electrons. This idea is relevant to a large number of model systems and materials [9–18]. Often, a small difference among the orbitals at the one-particle level is drastically amplified once many-body correlations are introduced. Importantly, a sharp localization-delocalization boundary can only be defined at zero temperature, in terms of the participation of the heavy charge carriers in the volume of the Fermi surface.

The OSMP has been investigated intensively using dynamical mean-field theory (DMFT) [19, 20] and slave-spin methods [21–23]. There is consensus that the OSMP is realized within these methods in the absence of hopping matrix elements between different orbitals [24]. This assumption is natural for local matrix elements (which are zero in high-symmetry situations [31]) but not for nonlocal ones (which are allowed by symmetry) [35]. In fact, in realistic estimations of materials, the interorbital nonlocal hopping amplitudes are often of the same order as those of the light electrons [36].

Earlier attempts to study the OSMP in the presence of interorbital hopping t_{io} resulted in different pictures. Using slave spins, Refs. [34, 39] concluded that the OSMP survives finite t_{io} at zero temperature, $T = 0$, while LDA+DMFT calculations of FeTe using a Monte Carlo impurity solver [40] argued in favor of a smooth crossover, where localization occurs only at

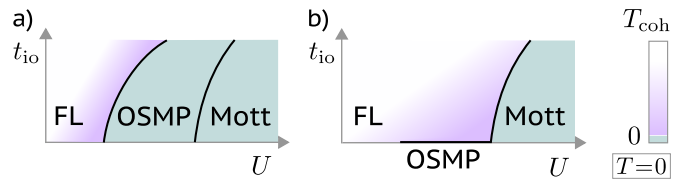


FIG. 1. Two possible scenarios, a) and b), for the zero-temperature ($T = 0$) phase diagram of multiorbital systems as a function of Coulomb repulsion U and interorbital hopping t_{io} . Here, we provide evidence for scenario b) in which any finite t_{io} replaces the OSMP by a Fermi liquid (FL). The coherence scale T_{coh} , below which all electrons are itinerant, is very low close to the OSMP and Mott phase.

sufficiently high T [41]. These two pictures are sketched in the qualitative $T = 0$ phase diagrams of Fig. 1. They also lead to different behavior for physical quantities at finite temperature: In the first case, one expects definite scaling behavior tied to a coherence scale T_{coh} which vanishes when a control parameter x (e.g., interaction strength or doping) reaches a critical value x_c . But the second scenario predicts a coherence-incoherence crossover where there is no such x_c and T_{coh} stays finite.

In this Letter, we settle this issue within the paramagnetic single-site DMFT in favor of the second scenario. We provide analytic arguments why any finite t_{io} destabilizes the OSMP, based on the form of the DMFT equations. The underlying mechanism has a simple physical interpretation, and we show that the same mechanism is obstructed within the more approximate slave-spin methods (thus explaining the results of Refs. [34, 39]). We obtain an exact numerical solution of the DMFT equations for a multiorbital model with interorbital hopping using the numerical renormalization group (NRG) [44]. This method is necessary to reach arbitrarily low T and to show that T_{coh} , while always finite, can be extremely small.

The basic argument goes as follows: the DMFT views correlated systems as a collection of atoms, each of which hybridizes with the environment given by the rest of the lattice. This hybridization plays a key role: taken at low energies, it is generically finite for Fermi liquids and vanishes for Mott

insulators. We will show that the low-energy hybridization of an electron in any orbital is finite as long as there is a finite amplitude for hopping to another, delocalized orbital and back. The only ingredients to this process are the momentum-dependent interorbital hopping $\epsilon_{\mathbf{k}}^{\text{io}}$ and the momentum- and frequency-dependent density of states $\mathcal{A}_{\mathbf{k}\nu}^{\text{lt}}$ of the light orbital, in the form $\sum_{\mathbf{k}} (\epsilon_{\mathbf{k}}^{\text{io}})^2 \mathcal{A}_{\mathbf{k}\nu}^{\text{lt}}$. It is this low-energy hybridization which destabilizes the Mott state in favor of a Fermi-liquid ground state. In the following, we first derive the hybridization formula for a two-orbital model, discuss the coherence scale, and then illustrate the consequences with numerical results.

Model—We consider a multiorbital Hubbard Hamiltonian

$$\hat{H} = \sum_{ijnm\sigma} \hat{d}_{in\sigma}^\dagger h_{ij}^{nm} \hat{d}_{jm\sigma} + \sum_i \hat{H}_{\text{int}}[\hat{d}_{in\sigma}], \quad (1)$$

where $\hat{d}_{in\sigma}^\dagger$ creates an electron at site i , in orbital n , and with spin σ . The hopping matrix h_{ij}^{nm} features nonlocal ($i \neq j$) interorbital ($n \neq m$) hopping; its Fourier transform is $h_{\mathbf{k}}^{nm}$. \hat{H}_{int} denotes the local interaction. In single-site DMFT, correlations are assumed to be local [19]. The propagator reads $\mathbf{G}_{\mathbf{k}\nu} = [\nu + \mu - \mathbf{h}_{\mathbf{k}} - \Sigma_{\nu}]^{-1}$ with the chemical potential μ and the retarded, matrix-valued self-energy Σ_{ν} . In sufficiently symmetric situations, the orbitals can be chosen such that local one-particle objects are diagonal in orbital space. This includes $\mathbf{G}_{\text{loc},\nu} = \sum_{\mathbf{k}} \mathbf{G}_{\mathbf{k}\nu}$ and Σ_{ν} just like the on-site energies $\epsilon_d = \sum_{\mathbf{k}} \mathbf{h}_{\mathbf{k}} - \mu$. Momentum sums are normalized: $\sum_{\mathbf{k}} 1 = 1$.

A minimal model for the OSMP has two orbitals, a light (lt) and a heavy (hv) orbital. We write the general hopping matrix, including the interorbital hopping $\epsilon_{\mathbf{k}}^{\text{io}}$, as

$$\mathbf{h}_{\mathbf{k}} - \mu = \begin{pmatrix} \epsilon_{\mathbf{k}}^{\text{lt}} & \epsilon_{\mathbf{k}}^{\text{io}} \\ \epsilon_{\mathbf{k}}^{\text{io}} & \epsilon_{\mathbf{k}}^{\text{hv}} \end{pmatrix}, \quad (2)$$

The local propagator follows from a 2×2 matrix inversion as

$$\mathbf{G}_{\text{loc},\nu} = \sum_{\mathbf{k}} \frac{1}{\prod_{n=\text{lt,hv}} [\nu - \epsilon_{\mathbf{k}}^n - \Sigma_{\nu}^n] - (\epsilon_{\mathbf{k}}^{\text{io}})^2} \times \begin{pmatrix} \nu - \epsilon_{\mathbf{k}}^{\text{hv}} - \Sigma_{\nu}^{\text{hv}} & -\epsilon_{\mathbf{k}}^{\text{io}} \\ -\epsilon_{\mathbf{k}}^{\text{io}} & \nu - \epsilon_{\mathbf{k}}^{\text{lt}} - \Sigma_{\nu}^{\text{lt}} \end{pmatrix}. \quad (3)$$

Diagonality of ϵ_d and $\mathbf{G}_{\text{loc},\nu}$ is ensured by a symmetry transformation $\mathbf{k} \rightarrow \mathbf{k}'$ among the momenta in the Brillouin zone with $\epsilon_{\mathbf{k}'}^n = \epsilon_{\mathbf{k}}^n$ ($n = \text{lt, hv}$) and $\epsilon_{\mathbf{k}'}^{\text{io}} = -\epsilon_{\mathbf{k}}^{\text{io}}$. Examples for such transformations are reflections $k_{\alpha} \rightarrow -k_{\alpha}$ ($\alpha = x, y, z$) or rotations like $(k_x, k_y) \rightarrow (k_y, -k_x)$ [45]. In our numerical computations, we use the simplistic expressions

$$\begin{aligned} \epsilon_{\mathbf{k}}^n &= -2t_n [\cos(k_x) + \cos(k_y) + \cos(k_z)] - \mu, \\ \epsilon_{\mathbf{k}}^{\text{io}} &= -2t_{\text{io}} [\cos(k_x) - \cos(k_y)]. \end{aligned} \quad (4)$$

DMFT equations—In DMFT, the lattice model is mapped onto an impurity model. We call the (orbital-diagonal) impurity propagator $\mathbf{g}_{\nu} = [\nu - \epsilon_d - \Delta_{\nu} - \Sigma_{\nu}]^{-1}$, where Δ_{ν} is the retarded hybridization function. The appropriate Δ_{ν} is found by iteration until self-consistency between the local lattice propagator and its impurity counterpart, $\mathbf{G}_{\text{loc},\nu} = \mathbf{g}_{\nu}$, is reached.

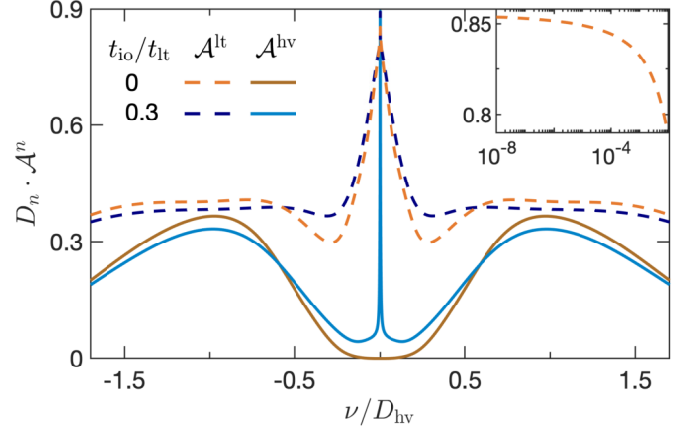


FIG. 2. Spectral functions \mathcal{A}^n for the light and heavy orbital. At $t_{\text{io}} = 0$, we find an OSMP with \mathcal{A}^{hv} gapped. Finite t_{io} destabilizes the OSMP as \mathcal{A}^{hv} develops a thin quasiparticle peak. Inset: In the OSMP, $\lim_{\nu \rightarrow 0} \mathcal{A}_{\nu}^{\text{lt}}$ converges only asymptotically [30, 48].

The diagonal elements of the local propagator are ($m \neq n$)

$$G_{\text{loc},\nu}^n = \sum_{\mathbf{k}} \frac{1}{r_{\mathbf{k}\nu}^n - \Sigma_{\nu}^n}, \quad r_{\mathbf{k}\nu}^n = \nu - \epsilon_{\mathbf{k}}^n - \frac{(\epsilon_{\mathbf{k}}^{\text{io}})^2}{\nu - \epsilon_{\mathbf{k}}^m - \Sigma_{\nu}^m}, \quad (5)$$

as taken from Eq. (3). From these, the hybridization in the bare impurity propagator is determined according to $G_{\text{loc},\nu}^n = g_{\nu}^n$. With $1/g_{0,\nu}^n = \nu - \epsilon_d^n - \Delta_{\nu}^n$, Δ_{ν}^n can be found from

$$\frac{1}{g_{0,\nu}^n} = \Sigma_{\nu}^n + \frac{1}{G_{\text{loc},\nu}^n} = \frac{\sum_{\mathbf{k}} \frac{r_{\mathbf{k}\nu}^n}{r_{\mathbf{k}\nu}^n - \Sigma_{\nu}^n}}{\sum_{\mathbf{k}} \frac{1}{r_{\mathbf{k}\nu}^n - \Sigma_{\nu}^n}}. \quad (6)$$

This intermediate result is key for the following discussion. It gives the hybridization components for a general two-orbital system [Eq. (2)] according to the DMFT self-consistency condition. We reshuffled the self-energy from the numerator into the denominator, but no approximation was made thus far.

While Eq. (6) holds at self-consistency, during the DMFT iteration, it is used to update Δ_{ν}^n from a given solution of the impurity model (yielding Σ_{ν}^n) to the next. We can briefly check the noninteracting case, $\Sigma_{\nu}^n = 0$, for which DMFT self-consistency is trivial. There, Eq. (6) correctly yields $g_{0,\nu}^n = \sum_{\mathbf{k}} \frac{1}{r_{\mathbf{k}\nu}^n}$. Next, we use Eq. (6) to investigate whether the OSMP is stable against interorbital hopping. To this end, we start from a converged DMFT solution with $t_{\text{io}} = 0$ realizing the OSMP. Then, we turn on t_{io} to check if the Mott insulator persists.

Indeed, starting at $t_{\text{io}} = 0$ and setting, e.g., $t_{\text{hv}} \ll t_{\text{lt}}$ at large interaction and half filling, the heavy orbital is Mott-insulating while the light orbital remains metallic. The Mott insulator is signaled by a gap in the local density of states $\mathcal{A}_{\nu}^{\text{hv}}$, where $-\pi \mathcal{A}_{\nu}^{\text{hv}} = \text{Im } G_{\text{loc},\nu}^n = \text{Im } g_{\nu}^n$, and a divergent effective mass, i.e., $\lim_{\nu \rightarrow 0} |\Sigma_{\nu}^{\text{hv}}| = \infty$. The impurity solution yielding \mathbf{g}_{ν} and Σ_{ν} is determined by the hybridization Δ_{ν} with spectral weights $\mathcal{A}_{\Delta,\nu}^n = -\text{Im } \Delta_{\nu}^n / \pi$. In most cases [11, 49–52], a Fermi-liquid ground state is found if all $\mathcal{A}_{\Delta,\nu}^n$ are finite around $\nu = 0$, while a Mott-insulating orbital requires a gapped $\mathcal{A}_{\Delta,\nu}^n$.

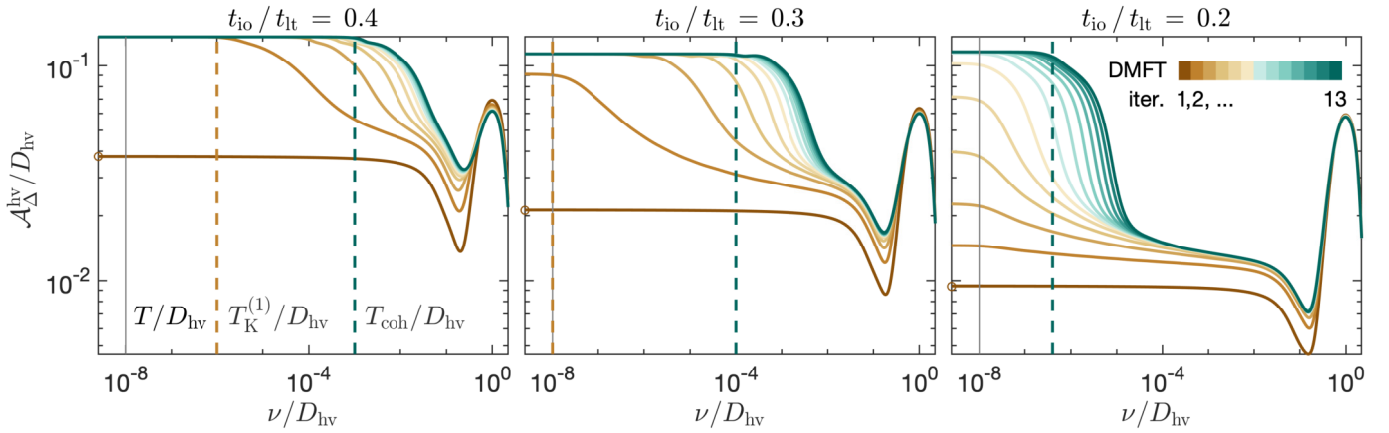


FIG. 3. Hybridization function \mathcal{A}_Δ in the heavy orbital for several DMFT iterations with finite t_{io} , starting from the OSMP solution at $t_{io}=0$. Circles on the vertical axis give values $(t_{io}/t_{lt})^2 \times \text{const}$ according to Eq. (7). Dashed vertical lines indicate the coherence scale after the first DMFT iteration, $T_K^{(1)}$, and after the last DMFT iteration, T_{coh} . For $t_{io}/t_{lt}=0.2$, $T_K^{(1)} \ll T$ and $T_{coh} \gtrsim T$; this opens a window of intermediate energies $|\nu| > T_{coh}$ with OSMP-like features (cf. Fig. 4).

Now, we perform the first DMFT update, starting from the OSMP solution but setting $t_{io} \neq 0$. It is clear from Eq. (5) that $\lim_{\nu \rightarrow 0} |\Sigma_\nu^{\text{hv}}| = \infty$ makes $G_{\text{loc},\nu=0}^n$ for both n independent of ϵ_k^{io} , so that, in particular, $\mathcal{A}_\nu^{\text{hv}}$ remains gapped. However, the result of the next iteration is determined by \mathcal{A}_Δ^n , not \mathcal{A}^n . The divergent self-energy also simplifies the updated hybridization function. In the limit $\nu \rightarrow 0$ within the OSMP, Eq. (6) yields

$$|\Sigma_\nu^{\text{hv}}| \rightarrow \infty: \frac{1}{g_{0,\nu}^{\text{hv}}} = \sum_k r_k^{\text{hv}}, \quad \Delta_\nu^{\text{hv}} = \sum_k (\epsilon_k^{\text{io}})^2 G_{k\nu}^{\text{lt}}. \quad (7)$$

For the second relation, $\nu - \epsilon_d^{\text{hv}}$ in $1/g_{0,\nu}^{\text{hv}}$ and $\sum_k (\nu - \epsilon_k^{\text{hv}})$ from r_k^{hv} cancel, and $G_{k\nu}^{\text{lt}} = 1/(\nu - \epsilon_k^{\text{lt}} - \Sigma_\nu^{\text{hv}})$ when Σ_ν^{hv} diverges. Equation (7) is the main result of our work. Assuming a divergent Σ_ν^{hv} for low frequencies, Δ_ν^{hv} retains a finite value, independent of Σ_ν^{hv} . Combining this with the fact that a finite hybridization leads to a Fermi-liquid ground state in fairly general impurity models [11, 49–52], we find that, with $\mathcal{A}_{\Delta,\nu}^{\text{hv}} = \sum_k (\epsilon_k^{\text{io}})^2 \mathcal{A}_{k\nu}^{\text{lt}} > 0$, the Mott insulating state of the heavy orbital is unstable against interorbital hopping. In further DMFT iterations, a quasiparticle peak in the heavy orbital will form, and Σ_ν^{hv} will no longer diverge. In Ref. [53], we show that Eq. (7) holds analogously for any number of orbitals.

We next include a temperature or energy coherence scale and estimate below which scale the Fermi-liquid properties are found. In the single-impurity Anderson model with a large interaction U and a (non-singular) hybridization \mathcal{A}_Δ , the coherence scale is the Kondo temperature T_K scaling exponentially with $U/\mathcal{A}_{\Delta,\nu=0}$ [54]. A similar behavior is expected for our model, albeit it with an effective \tilde{U} encoding further microscopic parameters (like Hund's coupling J) [55]. Now, for the first DMFT iteration after switching from $t_{io}=0$ to $t_{io} \neq 0$, we have $\mathcal{A}_{\Delta,\nu=0}^{\text{hv}} \propto t_{io}^2/t_{lt}$ from Eq. (7) and thus $T_K^{(1)} \propto \exp[-\alpha \tilde{U} t_{lt}/t_{io}^2] = c^{(t_{lt}/t_{io})^2}$, with a small constant $c \propto \exp[-\alpha \tilde{U}/t_{lt}]$ reminiscent of a single-orbital Kondo scale. This shows that the coherence scale for the first DMFT iteration after the OSMP can be extremely small. In the next iterations,

Σ_ν^{hv} is no longer divergent, and $\mathcal{A}_{\Delta,\nu=0}^{\text{hv}}$ cannot be deduced as easily. However, it is clear that delocalization of the heavy orbital will open more hybridization channels, so that $T_K^{(1)}$ serves as a lower bound for the actual coherence scale after DMFT convergence, $T_{coh} \geq T_K^{(1)}$.

Numerical results—We now turn to numerical results for the model of Eqs. (1), (2) and (4). We denote the half-bandwidth of ϵ_k^n by $D_n = 6t_n$ and consider two half-filled orbitals with $D_{lt}/D_{hv} = 2$. Using $D_{hv} = 1$ as our energy unit, we set the temperature to $T = 10^{-8}$, while \hat{H}_{int} is given by the Kanamori Hamiltonian [57] with parameters $U = 2.4$ and $J = 0.4$ [11]. We use NRG as a real-frequency impurity solver for DMFT, assuming paramagnetism; computational details are in Ref. [53].

To set the stage, Fig. 2 shows two sets of spectral functions \mathcal{A}^n for different interorbital hopping. Our interaction parameters are chosen such that $t_{io}=0$ realizes the OSMP, where \mathcal{A}^{hv} has a gap while \mathcal{A}^{lt} has a peak at $\nu=0$. Coupled to unscreened magnetic moments, the metallic orbital at zero temperature behaves as a singular Fermi liquid [30, 48], where $\lim_{\nu \rightarrow 0} \mathcal{A}_\nu^{\text{lt}} = 0$. For finite t_{io} , \mathcal{A}^{hv} develops a narrow quasiparticle peak, replacing the OSMP by a Fermi-liquid ground state. Nevertheless, at larger energies $|\nu| \gtrsim 10^{-2}$, the two sets of spectral functions for $t_{io}=0$ and $t_{io} \neq 0$ are very similar. In particular, pronounced Hubbard bands in \mathcal{A}^{hv} exist in both phases [59].

Figure 3 illustrates our analytic argument for the instability of the OSMP. It shows $\mathcal{A}_\Delta^{\text{hv}}$ for several DMFT iterations with finite t_{io} starting from the OSMP solution at $t_{io}=0$. In the first iteration, $\mathcal{A}_{\Delta,\nu}^{\text{hv}} \propto (t_{io}/t_{lt})^2$ according to Eq. (7). The resulting metallic state leads to an increased hybridization for the next iteration. Its coherence scale (below which, e.g., \mathcal{A}_ν^n converge) roughly follows $T_K^{(1)} \propto c^{(t_{lt}/t_{io})^2}$. For $t_{io}/t_{lt}=0.2$, $T_K^{(1)} \ll T$, so that $\mathcal{A}_{\Delta,\nu}^{\text{hv}}$ for the next iteration converges below T only. In the subsequent DMFT iterations, the hybridization further builds up until the actual coherence scale $T_{coh} \geq T_K^{(1)}$ is established. For $t_{io}/t_{lt}=0.2$, $T_{coh} \gtrsim T$ is very low, and OSMP-like behavior is found for $|\nu| > T_{coh}$.

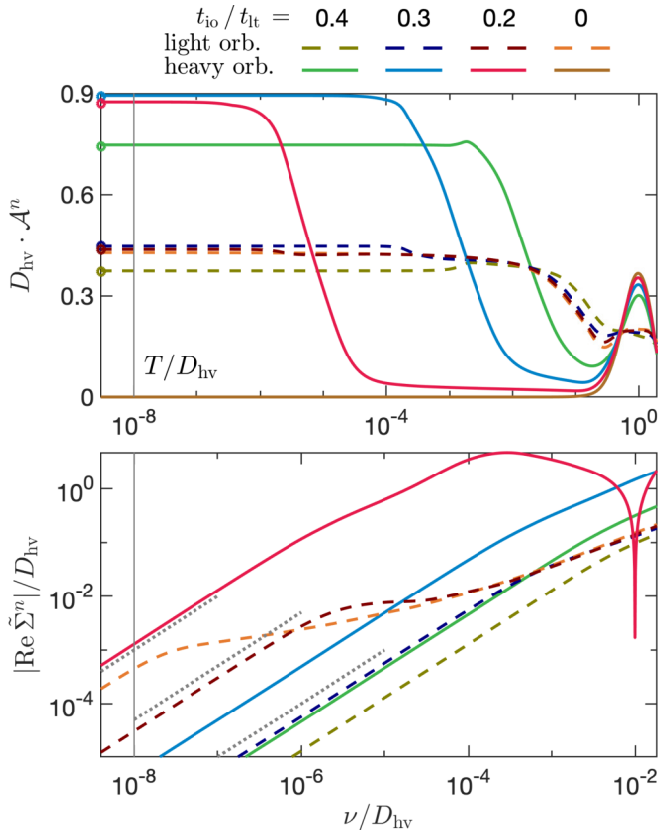


FIG. 4. Spectral functions \mathcal{A}_ν and self-energies $\tilde{\Sigma}_\nu = \Sigma_\nu - \Sigma_{\nu=0}$ after DMFT convergence. For $t_{\text{io}}/t_{\text{lt}} \in \{0.4, 0.3, 0.2\}$, Fermi-liquid behavior with $\mathcal{A}_{\nu=0}$ obeying Luttinger pinning (circles) and linear $\text{Re } \tilde{\Sigma}$ is seen below coherence scales of roughly 10^{-3} , 10^{-4} , and $4 \cdot 10^{-7}$, respectively (cf. Fig. 3). For $t_{\text{io}}/t_{\text{lt}} = 0.2$ and $10^{-5} < \nu/D_{\text{hv}} < 10^{-1}$, \mathcal{A}^{hv} almost vanishes and $\text{Re } \tilde{\Sigma}^{\text{lt}}$ perfectly follows the logarithmic behavior [30, 48] of the $t_{\text{io}} = 0$ OSMP. The three dotted lines indicate $\kappa\nu$, with $\kappa = 10^2, 5 \cdot 10^3, 10^5$ from bottom to top.

Indeed, Fig. 4 shows the spectral functions and self-energies after DMFT convergence. For all $t_{\text{io}} > 0$, a Fermi-liquid ground state is obtained, with a finite quasiparticle peak obeying Luttinger pinning [61] $\mathcal{A}_{\nu=0}^n = \rho_{\nu=0}^n$ and self-energies having a linear real part. At the lowest $t_{\text{io}} > 0$, however, both properties are fulfilled only at very low energies $|\nu| < T_{\text{coh}} \sim 4 \cdot 10^{-7}$ (even though \mathcal{A}^{lt} increases most strongly around $|\nu| \sim 10^{-1}$). For $|\nu| > T_{\text{coh}}$, the system is hardly distinguishable from the OSMP: in an intermediate regime of around four orders of magnitude, $\mathcal{A}_\nu^{\text{hv}}$ almost vanishes and Σ_ν^{lt} follows the logarithmic behavior of the OSMP [30, 48]. While the quasiparticle weights $Z_n = 1/(1 - \partial_\nu \text{Re } \Sigma_\nu|_{\nu=0})$ are already on the percent level for $t_{\text{io}}/t_{\text{lt}} = 0.3$, they reach values as low as 10^{-3} for the light and 10^{-5} for the heavy orbital at $t_{\text{io}}/t_{\text{lt}} = 0.2$. Decreasing t_{io} further, an OSMP is recovered as $T_{\text{coh}} < T = 10^{-8}$.

Comparison with slave spins—We finally compare our results to previous slave-spin studies which found the OSMP to be stable against interorbital hopping [39]. Slave-spin approaches decompose the physical fermions \hat{d} into a bosonic slave-spin operator \hat{b} and a slave fermion \hat{f}^\dagger , $\hat{d}_{im\sigma}^\dagger = \hat{b}_{im\sigma} \hat{f}_{im\sigma}^\dagger$. It was shown that the minimization of the mean-field decoupled free energy in slave-spin approaches is equivalent to a DMFT-

like treatment where the slave-spin impurity solver yields the quasiparticle weight and DMFT self-consistency is imposed on the slave fermions [34] [see their Eq. (30)].

Expressions for the f fermions are obtained from those of the d fermions by expanding the self-energy to linear order, $\Sigma_\nu^n \approx a_n + (1 - 1/Z_n)\nu$, and dividing out Z_n . For the local propagator [Eq. (5)], $G_{\text{loc},\nu}^{d,n} = Z_n G_{\text{loc},\nu}^{f,n}$, this yields ($m \neq n$)

$$G_{\text{loc},\nu}^{f,n} = \sum_{\mathbf{k}} \left[\nu - \epsilon_{\mathbf{k}}^{f,n} - \frac{(\epsilon_{\mathbf{k}}^{f,\text{io}})^2}{\nu - \epsilon_{\mathbf{k}}^{f,m}} \right]^{-1},$$

$$\epsilon_{\mathbf{k}}^{f,n} = Z_n(\epsilon_{\mathbf{k}}^{d,n} + a_n), \quad (\epsilon_{\mathbf{k}}^{f,\text{io}})^2 = Z_{\text{lt}} Z_{\text{hv}} (\epsilon_{\mathbf{k}}^{d,\text{io}})^2.$$

Due to the factor $Z_{\text{lt}} Z_{\text{hv}}$, the interorbital hopping has no effect here if $Z_{\text{hv}} = 0$. This agrees with our previous point that a dominant $|\Sigma_{\text{hv}}^{\text{hv}}|$ makes $G_{\text{loc},\nu}^{d,n}$ independent of $\epsilon_{\mathbf{k}}^{d,\text{io}}$. More insight is obtained from the impurity propagator, $g_\nu^{d,n} = Z_n g_\nu^{f,n}$, with

$$g_\nu^{f,n} = \frac{1}{\nu - \epsilon_f^n - \Delta_\nu^{f,n}}, \quad \epsilon_f^n = Z_n(\epsilon_d^n + a_n), \quad \Delta_\nu^{f,n} = Z_n \Delta_\nu^{d,n}.$$

One finds that the f -fermion self-consistency condition ($G_{\text{loc},\nu}^{f,n} = g_\nu^{f,n}$) leads to the same result for the d -fermion hybridization as in Eq. (7), now in the form $\Delta_\nu^{d,\text{hv}} = \sum_{\mathbf{k}} (\epsilon_{\mathbf{k}}^{d,\text{io}})^2 Z_{\text{lt}} C_{\mathbf{k}\nu}^{f,\text{lt}}$. This is still finite if the light orbital is metallic (here $Z_{\text{lt}} > 0$). However, the crucial difference lies in the fact that the impurity model for the slave spins is not characterized by Δ_ν^d but by Δ_ν^f . Here, each component is tied to the quasiparticle weight, $\Delta_\nu^{f,n} = Z_n \Delta_\nu^{d,n}$. Hence, if $Z_{\text{hv}} = 0$, the slave-spin impurity solver has no chance of seeing $\Delta_\nu^{d,\text{hv}} \neq 0$ and, thereby, no chance of generating $Z_{\text{hv}} > 0$ and leaving the OSMP. In other words, the inseparable connection of Z_n and $\Delta_\nu^{d,n}$ in slave-spin studies leads to additional extrema of the free energy which are not present in DMFT.

Conclusion—Using single-site DMFT, we showed that interorbital hopping t_{io} is a relevant perturbation to the OSMP and destabilizes it at $T = 0$ in favor of a Fermi-liquid ground state. The reason is that the low-energy hybridization in a given orbital has a finite contribution which stems from hopping to another orbital and back. Crucially, this term depends only on the availability of states in the intermediate orbital and not on the effective mass of the electron hopping. While an arbitrarily large imbalance in effective masses can still exist, within single-site DMFT, there is generically no OSMP with $t_{\text{io}} > 0$ at $T = 0$ and more generally below the coherence scale. Its finite-temperature properties may thus be viewed as a coherence–incoherence crossover, where selected orbitals are localized for $T > T_{\text{coh}}$ but itinerant for $T < T_{\text{coh}}$. This crossover can either be tuned by increasing T in a given system [4] or by decreasing T_{coh} at fixed (nonzero) T (as in [7]).

Our analytic arguments are supported by numerical results using NRG as a DMFT impurity solver, capable of accessing real frequencies and arbitrarily low temperatures. This allowed us to demonstrate that T_{coh} , below which the Fermi-liquid properties are found, is very sensitive to system parameters and can be extremely small, even for moderate values of $t_{\text{io}}/t_{\text{lt}}$.

We showed that many properties of the $t_{\text{io}} \neq 0$ state for energies above T_{coh} are almost indistinguishable from the $t_{\text{io}} = 0$ OSMP that reaches down to $T = 0$. Future theoretical work should aim to go beyond single-site DMFT to address the influence of non-local, interorbital self-energy components in renormalizing t_{io} [62]. Experimentally, our results can be tested by measuring the normal-state Fermi-surface volume at very low T and by analyzing the scaling behavior in the OSMP at $T > 0$.

Acknowledgments—We thank A. Weichselbaum and Seung-Sup B. Lee for a critical reading of the manuscript and K. Haule for discussions. The NRG results were obtained using the QSpace tensor library developed by A. Weichselbaum [63] and the NRG toolbox by Seung-Sup B. Lee [64, 65]. F. B. K. and G. K. acknowledge support by the NSF grant DMR-1733071. F. B. K. acknowledges support by the Alexander von Humboldt Foundation through the Feodor Lynen Fellowship.

[1] M. Imada, A. Fujimori, and Y. Tokura, *Rev. Mod. Phys.* **70**, 1039 (1998).

[2] P. A. Lee, N. Nagaosa, and X.-G. Wen, *Rev. Mod. Phys.* **78**, 17 (2006).

[3] Q. Si, R. Yu, and E. Abrahams, *Nat. Rev. Mater.* **1**, (2016).

[4] M. Yi, Z.-K. Liu, Y. Zhang, R. Yu, J.-X. Zhu, J. Lee, R. Moore, F. Schmitt, W. Li, S. Riggs, J.-H. Chu, B. Lv, J. Hu, M. Hashimoto, S.-K. Mo, Z. Hussain, Z. Mao, C. Chu, I. Fisher, Q. Si, Z.-X. Shen, and D. Lu, *Nat. Commun.* **6**, (2015).

[5] Z. K. Liu, M. Yi, Y. Zhang, J. Hu, R. Yu, J.-X. Zhu, R.-H. He, Y. L. Chen, M. Hashimoto, R. G. Moore, S.-K. Mo, Z. Hussain, Q. Si, Z. Q. Mao, D. H. Lu, and Z.-X. Shen, *Phys. Rev. B* **92**, 235138 (2015).

[6] T. Otsuka, S. Haga, Y. Koshika, S. Adachi, T. Usui, N. Sasaki, S. Sasaki, S. Yamaguchi, Y. Nakanishi, M. Yoshizawa, S. Kimura, and T. Watanabe, *Phys. Rev. B* **99**, 184505 (2019).

[7] J. Huang, R. Yu, Z. Xu, J.-X. Zhu, Q. Jiang, M. Wang, H. Wu, T. Chen, J. D. Denlinger, S.-K. Mo, M. Hashimoto, G. Gu, P. Dai, J.-H. Chu, D. Lu, Q. Si, R. J. Birgeneau, and M. Yi, *arXiv:2010.13913*.

[8] V. Anisimov, I. Nekrasov, D. Kondakov, T. Rice, and M. Sigrist, *Eur. Phys. J. B* **25**, 191 (2002).

[9] M. Neupane, P. Richard, Z.-H. Pan, Y.-M. Xu, R. Jin, D. Mandrus, X. Dai, Z. Fang, Z. Wang, and H. Ding, *Phys. Rev. Lett.* **103**, 097001 (2009).

[10] M. Vojta, *J. Low Temp. Phys.* **161**, 203 (2010).

[11] A. Georges, L. de' Medici, and J. Mravlje, *Annu. Rev. Condens. Matter Phys.* **4**, 137 (2013).

[12] F. Hardy, A. E. Böhmer, D. Aoki, P. Burger, T. Wolf, P. Schweiss, R. Heid, P. Adelmann, Y. X. Yao, G. Kotliar, J. Schmalian, and C. Meingast, *Phys. Rev. Lett.* **111**, 027002 (2013).

[13] Y. J. Pu, Z. C. Huang, H. C. Xu, D. F. Xu, Q. Song, C. H. P. Wen, R. Peng, and D. L. Feng, *Phys. Rev. B* **94**, 115146 (2016).

[14] H. Miao, Z. P. Yin, S. F. Wu, J. M. Li, J. Ma, B.-Q. Lv, X. P. Wang, T. Qian, P. Richard, L.-Y. Xing, X.-C. Wang, C. Q. Jin, K. Haule, G. Kotliar, and H. Ding, *Phys. Rev. B* **94**, 201109 (2016).

[15] N. Lanatà, Y. Yao, X. Deng, V. Dobrosavljević, and G. Kotliar, *Phys. Rev. Lett.* **118**, 126401 (2017).

[16] C.-W. Chen, W. Wang, V. Loganathan, S. V. Carr, L. W. Harriger, C. Georgen, A. H. Nevidomskyy, P. Dai, C.-L. Huang, and E. Morosan, *Phys. Rev. B* **99**, 144423 (2019).

[17] G. L. Pascut and K. Haule, *arXiv:2005.12179*.

[18] M. Kim, H.-S. Kim, K. Haule, and D. Vanderbilt, *arXiv:2106.06204*.

[19] A. Georges, G. Kotliar, W. Krauth, and M. J. Rozenberg, *Rev. Mod. Phys.* **68**, 13 (1996).

[20] G. Kotliar, S. Y. Savrasov, K. Haule, V. S. Oudovenko, O. Parcollet, and C. A. Marianetti, *Rev. Mod. Phys.* **78**, 865 (2006).

[21] L. de' Medici, A. Georges, and S. Biermann, *Phys. Rev. B* **72**, 205124 (2005).

[22] S. R. Hassan and L. de' Medici, *Phys. Rev. B* **81**, 035106 (2010).

[23] R. Yu and Q. Si, *Phys. Rev. B* **86**, 085104 (2012).

[24] Recent works are, e.g., Refs. [25–30].

[25] P. Werner, E. Gull, and A. J. Millis, *Phys. Rev. B* **79**, 115119 (2009).

[26] L. de' Medici, S. R. Hassan, M. Capone, and X. Dai, *Phys. Rev. Lett.* **102**, 126401 (2009).

[27] T. Kita, T. Ohashi, and N. Kawakami, *Phys. Rev. B* **84**, 195130 (2011).

[28] L. Huang, L. Du, and X. Dai, *Phys. Rev. B* **86**, 035150 (2012).

[29] Y. Wang, L. Huang, L. Du, and X. Dai, *Chin. Phys. B* **25**, 037103 (2016).

[30] F. B. Kugler, S.-S. B. Lee, A. Weichselbaum, G. Kotliar, and J. von Delft, *Phys. Rev. B* **100**, 115159 (2019).

[31] The effect of local interorbital hybridization on the OSMP is discussed in Refs. [21, 32–34].

[32] A. Koga, N. Kawakami, T. M. Rice, and M. Sigrist, *Phys. Rev. B* **72**, 045128 (2005).

[33] L. de' Medici, A. Georges, G. Kotliar, and S. Biermann, *Phys. Rev. Lett.* **95**, 066402 (2005).

[34] Y. Komijani and G. Kotliar, *Phys. Rev. B* **96**, 125111 (2017).

[35] J. C. Slater and G. F. Koster, *Phys. Rev.* **94**, 1498 (1954).

[36] See, e.g., Table A.4 in Ref. [37] for iron pnictides and Tables S1 and S2 in the Supplemental Material of Ref. [38] for FeSe.

[37] K. Haule and G. Kotliar, *New J. Phys.* **11**, 025021 (2009).

[38] R. Yu, J.-X. Zhu, and Q. Si, *Phys. Rev. Lett.* **121**, 227003 (2018).

[39] R. Yu and Q. Si, *Phys. Rev. Lett.* **110**, 146402 (2013); *Phys. Rev. B* **96**, 125110 (2017).

[40] Z. P. Yin, K. Haule, and G. Kotliar, *Phys. Rev. B* **86**, 195141 (2012).

[41] Note that Refs. [42, 43] argue for a stable OSMP in the presence of interorbital hopping using DMFT and a Lanczos impurity solver. They consider a two-orbital model with an identical real-space dependence of all hopping components and use a canonical transformation that kinetically decouples the two orbitals. This is, however, not the generic situation, and such a decoupling scheme is no longer possible once the intra- and interorbital hoppings have different momentum dependencies.

[42] Y. Song and L.-J. Zou, *Phys. Rev. B* **72**, 085114 (2005); *Eur. Phys. J. B* **72**, 59 (2009).

[43] Y. Ni, J. Sun, Y.-M. Quan, and Y. Song, *arXiv:2112.04664*.

[44] R. Bulla, T. A. Costi, and T. Pruschke, *Rev. Mod. Phys.* **80**, 395 (2008).

[45] For explicit tight-binding models of iron pnictides, see, e.g., Ref. [46, 47].

[46] K. Kuroki, S. Onari, R. Arita, H. Usui, Y. Tanaka, H. Kontani, and H. Aoki, *Phys. Rev. Lett.* **101**, 087004 (2008).

[47] S. Graser, T. A. Maier, P. J. Hirschfeld, and D. J. Scalapino, *New J. Phys.* **11**, 025016 (2009).

[48] M. Greger, M. Sekania, and M. Kollar, *arXiv:1312.0100*.

[49] A. C. Hewson, *The Kondo Problem to Heavy Fermions*, Cambridge Studies in Magnetism (Cambridge University Press, Cambridge, 1993).

[50] L. De Leo, *Non-Fermi liquid behavior in multi-orbital Anderson*

impurity models and possible relevance for strongly correlated lattice models, Ph.D. thesis, SISSA (2004).

[51] C. Aron and G. Kotliar, *Phys. Rev. B* **91**, 041110 (2015).

[52] E. Walter, K. M. Stadler, S.-S. B. Lee, Y. Wang, G. Kotliar, A. Weichselbaum, and J. von Delft, *Phys. Rev. X* **10**, 031052 (2020).

[53] See the Supplemental Material at [url] for computational details, the bare density of states, numerical results away from half filling, and analytic arguments for an arbitrary number of orbitals, which contains Refs. [66–70] listed below.

[54] Here, we use the standard formula for the Kondo temperature, $T_K = 0.4107 (U\Gamma/2)^{1/2} \exp(-\frac{\pi U}{8\Gamma} + \frac{\pi\Gamma}{2U})$, where $\Gamma = \pi\mathcal{A}_{\Delta,\nu=0}$; see Eq. (6.109) and the following text in Ref. [49].

[55] Apart from the details of the local Hamiltonian, in DMFT, there are interesting subtleties to the Kondo temperature following from the shape of the hybridization function [56]. Yet, for our discussion, the only important aspect is that the exponential factor $\exp[-1/(\rho_0 J)]$ with $J \sim t^2/U$ remains the same.

[56] K. Held, R. Peters, and A. Toschi, *Phys. Rev. Lett.* **110**, 246402 (2013).

[57] While we keep the spin-flip part of the Kanamori Hamiltonian, we neglect pair hopping in order to exploit charge conservation in each orbital. This can be justified *a posteriori* if the probability of finding an empty and a fully occupied orbital is very low [58].

[58] F. B. Kugler, M. Zingl, H. U. R. Strand, S.-S. B. Lee, J. von Delft, and A. Georges, *Phys. Rev. Lett.* **124**, 016401 (2020).

[59] Next to the Hubbard bands, the insulating spectral function of the OSMP generally also features interband doublon-holon excitations (DHEs) [30, 60]. Applying the techniques of Appendix B in Ref. [30] to our model, the Hubbard bands are centered at energies $\pm(U - J)/2 = \pm 1.4$ while the DHEs occur at $\pm 3J = \pm 1.2$. Hence, for the given parameters, the DHEs are placed deep within the Hubbard bands and are thus not discernible.

[60] Y. Núñez Fernández, G. Kotliar, and K. Hallberg, *Phys. Rev. B* **97**, 121113 (2018).

[61] E. Müller-Hartmann, *Z. Phys. B* **76**, 211 (1989).

[62] L. De Leo, M. Civelli, and G. Kotliar, *Phys. Rev. Lett.* **101**, 256404 (2008).

[63] A. Weichselbaum, *Ann. Phys.* **327**, 2972 (2012); *Phys. Rev. B* **86**, 245124 (2012); *Phys. Rev. Research* **2**, 023385 (2020).

[64] S.-S. B. Lee and A. Weichselbaum, *Phys. Rev. B* **94**, 235127 (2016).

[65] S.-S. B. Lee, J. von Delft, and A. Weichselbaum, *Phys. Rev. Lett.* **119**, 236402 (2017).

[66] A. Weichselbaum and J. von Delft, *Phys. Rev. Lett.* **99**, 076402 (2007).

[67] A. K. Mitchell, M. R. Galpin, S. Wilson-Fletcher, D. E. Logan, and R. Bulla, *Phys. Rev. B* **89**, 121105 (2014).

[68] K. M. Stadler, A. K. Mitchell, J. von Delft, and A. Weichselbaum, *Phys. Rev. B* **93**, 235101 (2016).

[69] R. Bulla, A. C. Hewson, and T. Pruschke, *J. Phys.: Condens. Matter* **10**, 8365 (1998).

[70] R. Žitko and T. Pruschke, *Phys. Rev. B* **79**, 085106 (2009).

Supplemental Material for “Is the orbital-selective Mott phase stable against interorbital hopping?”

Fabian B. Kugler¹ and Gabriel Kotliar^{1,2}

¹Department of Physics and Astronomy, Rutgers University, Piscataway, NJ 08854, USA

²Condensed Matter Physics and Materials Science Department, Brookhaven National Laboratory, Upton, NY 11973, USA

In this Supplemental Material, we provide the computational details of our study, additional figures for the (particle-hole symmetric) bare density of states and the spectral functions away from particle-hole symmetry, and generalize the central Eq. (7) of the main text to an arbitrary number of orbitals. Citations refer to the list of references given in the main text.

COMPUTATIONAL DETAILS

We employ the full density-matrix (fdm) NRG [66] and exploit the $U(1)_{lt} \times U(1)_{hv} \times SU(2)_{sp}$ charge and spin symmetries using the QSpace tensor library [63]. For further efficiency, the Wilson chain of both orbitals are interleaved [67, 68]. We use an NRG discretization parameter of $\Lambda = 4$ and keep up to 25000 $SU(2)$ -spin multiplets in the beginning of the iterative diagonalization and around 15000 at the end of it. The self-energy is obtained by an equation-of-motion trick [69]. The resolution at finite energies is improved by averaging results over two shifted discretization grids [70] and by using an adaptive broadening scheme [64, 65]. The DMFT iterations are performed until point-wise convergence of $\mathcal{A}_{\Delta,\nu}$ at the level of $10^{-4}D_{hv}$ is reached. Momentum sums are evaluated with more than $3 \cdot 10^7$ uniformly spaced momentum points in the irreducible Brillouin zone, while manually setting $-\text{Im} \Sigma_{\nu}^n \geq 0.004D_{hv}$ to obtain smooth curves.

ADDITIONAL FIGURES

Figure 5 shows the bare density of states for the system defined by Eqs. (2) and (4) of the main text at $\mu = 0$. In a Fermi-

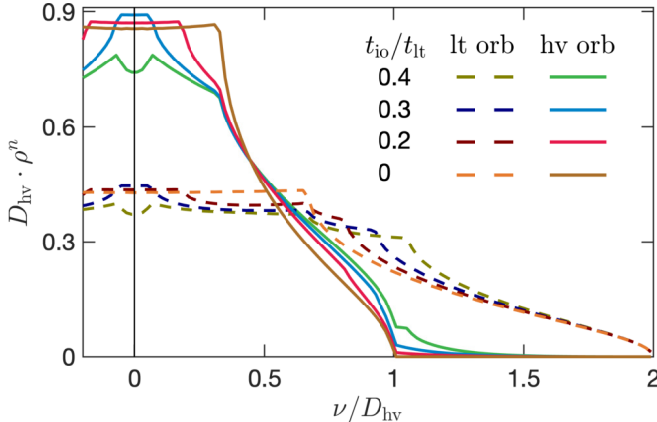


FIG. 5. The bare density of states ρ^n , i.e. the noninteracting hybridization function \mathcal{A}_{Δ}^n , for various interorbital hoppings t_{io}/t_{lt} .

liquid state, Luttinger pinning [61] dictates $\rho_{\nu=0}^n = \mathcal{A}_{\nu=0}^n$ at particle-hole symmetry.

Next, we discuss results away from particle-hole symmetry. To this end, we refine Eq. (4) from the main text as

$$\begin{aligned} \epsilon_{\mathbf{k}}^n &= -2t_n[\cos(k_x) + \cos(k_y) + \cos(k_z)] - \mu_n, \\ \epsilon_{\mathbf{k}}^{\text{io}} &= -2t_{\text{io}}[\cos(k_x) - \cos(k_y)], \end{aligned} \quad (\text{S1})$$

allowing for a crystal-field splitting $\Delta_{\text{cfs}} = \mu_{lt} - \mu_{hv}$. Indeed, while keeping equal hopping amplitudes $t_{lt} = t_{hv} = 1$, we use $\Delta_{\text{cfs}} \neq 0$ to induce orbital differentiation and an imbalance in the effective masses. For $\Delta_{\text{cfs}} = 0.875$ and a suitable average chemical potential $(\mu_{lt} + \mu_{hv})/2$, the heavy orbital is close to half filling whereas the light orbital is close to quarter filling. Furthermore, we here choose interaction parameters $U = 3$ and $J = 0.5$.

Figure 6 presents our results away from particle-hole symmetry in a way analogous to Fig. 2 of the main text. Without interorbital hopping, $t_{io}=0$, the system is an OSMP: the spectral function of the heavy orbital is gapped while that of the light orbital converges asymptotically to a finite value $\mathcal{A}_{\nu=0}^{\text{lt}}$ (see inset). Again, the OSMP is unstable against interorbital hopping and, for $t_{io}/t_{lt} = 0.5$, a quasiparticle peak in the heavy orbital develops. Indeed, our analytic arguments on the instability of the OSMP against interorbital hopping given in the main text are very general and independent of fillings or crystal fields. We checked numerically that all statements regarding the build up of the hybridization in the heavy orbital, the low coherence scale T_{coh} , and the OSMP-like properties for $|\nu| > T_{\text{coh}}$ also hold in this particle-hole asymmetric setup.

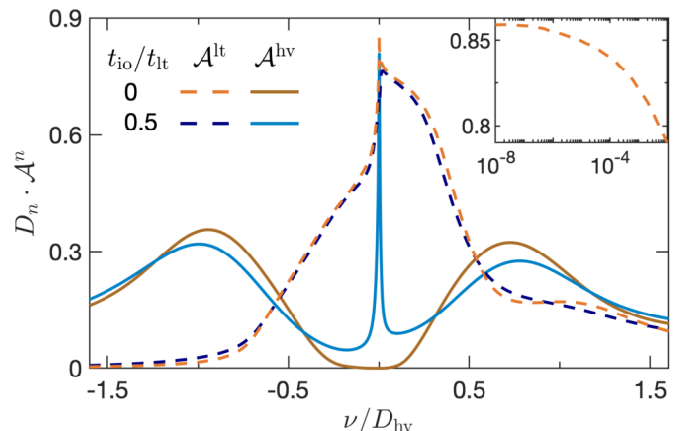


FIG. 6. Spectral functions \mathcal{A}^n for the light and heavy orbital, similarly as in Fig. 2 of the main text, but away from particle-hole symmetry.

ANY NUMBER OF ORBITALS

We start from the DMFT self-consistency condition in the form $\mathbf{g}_\nu = \mathbf{G}_{\text{loc},\nu}$, where \mathbf{g}_ν is diagonal with components $1/g_\nu^n = \nu - \epsilon_d^n - \Delta_\nu^n - \Sigma_\nu^n$ and $\mathbf{G}_{\text{loc},\nu} = \sum_{\mathbf{k}} (\nu + \mu - \mathbf{h}_\mathbf{k} - \Sigma_\nu)^{-1}$. Next, we define a new, orbital-diagonal variable

$$\mathbf{S}_\nu = \nu - \epsilon_d - \Sigma_\nu. \quad (\text{S2})$$

This allows us to write $1/g_\nu^n = S_\nu^n - \Delta_\nu^n$, as well as $\mathbf{G}_{\text{loc},\nu} = 1/(S_\nu - \tilde{\mathbf{h}}_\mathbf{k})^{-1}$ with the purely nonlocal hopping matrix

$$\tilde{\mathbf{h}}_\mathbf{k} = \mathbf{h}_\mathbf{k} - \mu - \epsilon_d, \quad \sum_{\mathbf{k}} \tilde{\mathbf{h}}_\mathbf{k} = 0. \quad (\text{S3})$$

Now, we assume again that the self-energy of one orbital n (the ‘‘heavy’’ orbital) diverges at low energies, $\lim_{\nu \rightarrow 0} |\Sigma_\nu^n| = \infty$, and we expand the DMFT self-consistency condition in $1/|\Sigma_\nu^n|$. We take the nn component of $\mathbf{g}_\nu = \mathbf{G}_{\text{loc},\nu}$,

$$\frac{1}{S_\nu^n - \Delta_\nu^n} = \left[\sum_{\mathbf{k}} (S_\nu - \tilde{\mathbf{h}}_\mathbf{k})^{-1} \right]_{nn}. \quad (\text{S4})$$

Next, we subtract the leading $1/S_\nu^n$ part as

$$\frac{1}{S_\nu^n - \Delta_\nu^n} - \frac{1}{S_\nu^n} = \left[\sum_{\mathbf{k}} (S_\nu - \tilde{\mathbf{h}}_\mathbf{k})^{-1} - S_\nu^{-1} \right]_{nn}. \quad (\text{S5})$$

This gives $\Delta_\nu^n / [(S_\nu^n - \Delta_\nu^n) S_\nu^n]$ on the left of Eq. (S5) and

$$\begin{aligned} & \left[\sum_{\mathbf{k}} (S_\nu - \tilde{\mathbf{h}}_\mathbf{k})^{-1} (1 - (S_\nu - \tilde{\mathbf{h}}_\mathbf{k}) S_\nu^{-1}) \right]_{nn} \\ &= \left[\sum_{\mathbf{k}} (S_\nu - \tilde{\mathbf{h}}_\mathbf{k})^{-1} \tilde{\mathbf{h}}_\mathbf{k} S_\nu^{-1} \right]_{nn} \end{aligned} \quad (\text{S6})$$

on the right. Finally, we multiply by S_ν on both sides to extract Δ_ν^n . Indeed, on the left of Eq. (S5), we get

$$S_\nu^n \Delta_\nu^n / (S_\nu^n - \Delta_\nu^n) = \Delta_\nu^n + O(\Delta_\nu^n / S_\nu^n).$$

Starting from Eq. (S6), the right side is obtained as

$$\left[\sum_{\mathbf{k}} S_\nu (S_\nu - \tilde{\mathbf{h}}_\mathbf{k})^{-1} \tilde{\mathbf{h}}_\mathbf{k} \right]_{nn} = \left[\sum_{\mathbf{k}} \tilde{\mathbf{h}}_\mathbf{k} (S_\nu - \tilde{\mathbf{h}}_\mathbf{k})^{-1} \tilde{\mathbf{h}}_\mathbf{k} \right]_{nn}.$$

For the last step, we rewrote S_ν as $S_\nu - \tilde{\mathbf{h}}_\mathbf{k} + \tilde{\mathbf{h}}_\mathbf{k}$ and used that $\sum_{\mathbf{k}} \tilde{\mathbf{h}}_\mathbf{k} = 0$ [see Eq. (S3)].

We thus find the generalization of Eq. (7) of the main text as

$$\begin{aligned} \Delta_\nu^n &= \left[\sum_{\mathbf{k}} \tilde{\mathbf{h}}_\mathbf{k} \mathbf{G}_{\mathbf{k}\nu} \tilde{\mathbf{h}}_\mathbf{k} \right]_{nn} + O(\Delta_\nu^n / S_\nu^n) \\ &= \sum_{\mathbf{k}} \sum_{m, m' \neq n} h_{\mathbf{k}}^{nm} G_{\mathbf{k}\nu}^{mm'} h_{\mathbf{k}}^{m'n} + O(\Delta_\nu^n / S_\nu^n). \end{aligned} \quad (\text{S7})$$

For the last step, we used that $G_{\mathbf{k}\nu}^{nn} \in O(1/S_\nu^n)$ and that $\tilde{\mathbf{h}}_\mathbf{k}^{nm} = h_{\mathbf{k}}^{nm}$ for $n \neq m$ since μ and ϵ_d in Eq. (S3) are diagonal.